Eur J Plant Pathol (2009) 125:291–302
DOI 10.1007/s10658-009-9482-7

Pre-symptomatic detection of *Plasmopara viticola* infection in grapevine leaves using chlorophyll fluorescence imaging

Ladislav Cséfalvay · Gabriele Di Gaspero · Karel Matouš · Diana Bellin · Benedetto Ruperti · Julie Olejníčková

Received: 20 January 2009 / Accepted: 16 April 2009 / Published online: 29 April 2009

Abstract *Plasmopara viticola* is an economically important pathogen of grapevine. Early detection of *P. viticola* infection can lead to improved fungicide treatment. Our study aimed to determine whether chlorophyll fluorescence (Chl-F) imaging can be used to reveal early stages of *P. viticola* infection under conditions similar to those occurring in commercial vineyards. Maximum (F_V/F_M) and effective quantum yield of photosystem II (Φ_{PSII}) were identified as the most sensitive reporters of the infection. Heterogeneous distribution of F_V/F_M and Φ_{PSII} in artificially inoculated leaves was associated with the presence of the developing mycelium 3 days before the occurrence of visible symptoms and 5 days before the release of spores. Significant changes of F_V/F_M and Φ_{PSII} were spatially coincident with localised spots of inoculation across the leaf lamina. Reduction of F_V/F_M was restricted to the leaf area that later yielded sporulation, while the area with significantly lower Φ_{PSII} was larger and probably reflected the leaf parts in which photosynthesis was impaired. Our results indicate that Chl-F can be used for the early detection of *P. viticola* infection. Because *P. viticola* does not expand systemically in the host tissues and the effects of infection are localised, Chl-F imaging at high resolution is necessary to reveal the disease in the field.

L. Cséfalvay (✉) · K. Matouš · J. Olejníčková
Laboratory of Physiology and Ecology,
Department of Biological Dynamics,
Institute of Systems Biology and Ecology,
Academy of Sciences of the Czech Republic,
Zámek 136,
CZ-37333 Nové Hrady, Czech Republic
e-mail: csefalvay@nh.usbe.cas.cz

L. Cséfalvay · K. Matouš · J. Olejníčková
Department of Systems Biology,
Institute of Physical Biology, University of South Bohemia,
Zámek 136,
CZ-37333 Nové Hrady, Czech Republic

G. Di Gaspero · D. Bellin · B. Ruperti
Dipartimento di Scienze Agrarie e Ambientali,
University of Udine,
via delle Scienze 208,
33100 Udine, Italy

G. Di Gaspero
Istituto di Genomica Applicata,
Parco Scientifico e Tecnologico Luigi Danieli,
via Jacopo Linussio 51,
33100 Udine, Italy

Present Address:
B. Ruperti
Dipartimento di Agronomia Ambientale e Produzioni Vegetali, University of Padua,
viale dell'Università 16, Legnaro,
35122 Padua, Italy

Keywords Biotic stress · Combinatorial imaging · Fungal infection · Mildew disease · Pest management · *Vitis vinifera*

Abbreviations

CCD	charged coupled device
Chl-F	chlorophyll fluorescence
CI	combinatorial imaging

dpi	days post-inoculation
F_0	minimum chlorophyll fluorescence yield in dark-adapted state
F_M	maximum chlorophyll fluorescence yield in dark-adapted state
$F_{M1`}$ $F_{M2`}$, $F_{M3`}$, F_{M4}	maximum chlorophyll fluorescence yield in light-adapted state measured in 1st, 2nd, 3rd and 4th saturating pulse
F_V	variable chlorophyll fluorescence yield in dark-adapted state
F_P	maximum chlorophyll fluorescence yield measured when the actinic light is switched on
F_S	steady-state chlorophyll fluorescence yield in light-adapted state
F_t	actual chlorophyll fluorescence yield at a particular time
F_V/F_M	maximum quantum yield of photosystem II photochemistry
Φ_{PSII}	effective quantum yield of photosystem II photochemistry
HL	high light
IF	infected area
LED	Light Emitting Diode
LL	low light
MIF	mesophyll-invaded area
NIF	non-infected area
PSII	photosystem II
NPQ	non-photochemical quenching of chlorophyll fluorescence

Introduction

Fungal diseases endanger grapevine yield and cause significant economic losses. In order to protect grapevines in the European Union (EU), approximately 60,000 tons of active substances (65% of all fungicides used in the EU) are distributed over 3.5 million ha of vineyards planted with susceptible cultivars of *Vitis vinifera*, which represent only 3.3% of the agricultural acreage in the EU (Eurostat report 2007). Strict regulations were adopted to reduce the input of chemicals in pest management programmes (European Community Regulation 473/2002). Biofungicides used in organic farming are an alternative approach to disease control, but they do not prevent mildews satisfactorily under high disease pressure (Spera et al. 2003; La Torre et al. 2005). The foundation of sustainable viticulture relies either on the replacement of traditional varieties with new genetic material having resistance genes that prevent pathogen colonisation (Jaillon et al. 2007), or on the introduction of methods for detecting infection at the initial stages and therefore reducing fungicide applications to the minimum level of necessity.

The oomycete *Plasmopara viticola* is the causal agent of downy mildew, the most damaging fungal disease in cool climates (optimum 20°–25°C, extremes 10°–29°C) with abundant rains in late spring, as are most of the European vineyards that fall short of the Mediterranean regions (Emmett et al. 1992). This pathogen impairs leaf physiology soon after the onset of infection (Polesani et al. 2008). In the following 5–15 days depending on the environmental conditions, *P. viticola* grows within the leaf tissue and causes significant economic loss if no chemicals are applied. Zoospore germination and tissue penetration by *P. viticola* are triggered during the vegetative growth of the vine, whenever rainfalls cause the abaxial surface of leaves to remain wet for at least 2 h. The steady-state environment and physiological conditions, which are somewhat predictable, influence the successful development of mycelium and, eventually, sporulation. Vine growers usually prevent the disease by spraying at any time they foresee favourable meteorological conditions for pathogen outbreak. Forecasting models have contributed to the abandonment of calendar sprayings. However, these simulators often alert growers to treat vines in the absence of infection, which leads to the wasting of chemicals and money (Bugliosi et al. 2007). Rapid tools for monitoring the presence and the severity of the infection in the vineyard, before the symptoms appear, would help growers to confirm or disregard the alert of forecasting models, and to apply chemicals more sparingly, without the risk of crop loss.

Visualisation of the infections at pre-symptomatic stages can be achieved by imaging of the heterogeneous distribution of various plant optical signals. One of them is chlorophyll fluorescence emission (Chl-F), which has been frequently used for the early detection of biotic stress before the occurrence of visible symptoms (e.g., Chaerle and Van Der Straeten 2001; Barbagallo et al. 2003; Nedbal and Whitmarsh 2004). Since many pathogens interfere with the host

metabolism by inducing changes in the photosynthetic process (e.g., Chou et al. 2000; Meyer et al. 2001; Soukupová et al. 2003; Scharte et al. 2005; Berger et al. 2007; Rodríguez-Moreno et al. 2008), these changes can be tracked by imaging Chl-F fluctuations in infected tissues (Omasa et al. 1987; Lichtenthaler and Miehé 1997; Nedbal and Whitmarsh 2004). Chl-F variations are particularly useful for the early detection of fungal infections (e.g., Scholes and Rolfe 1996; Chou et al. 2000; Swarbrick et al. 2006). Chl-F is capable of revealing the physiological alteration of photosynthesis, because Chl-F emission is one of the three pathways of light energy de-excitation and, hence, it is inversely correlated with photochemistry, which leads to CO_2 assimilation, and with heat dissipation (reviewed by e.g., Papageorgiou and Govindjee 2004). The competition between photosynthesis and Chl-F makes Chl-F a suitable non-invasive reporter of photosynthetic activity.

The aim of this study was to investigate possibilities of the early detection of *P. viticola* infection in grapevine using Chl-F imaging, with particular attention to Chl-F parameters that correlate with leaf photosynthetic activity (F_V/F_M and Φ_{PSII}, maximum and effective quantum yield of photosystem II (PSII), respectively; Kitajima and Butler 1975; Genty et al. 1989) and are best suited for field measurements. Although these Chl-F parameters are directly linked to physiological changes occurring in infected tissues, they do not necessarily provide the best diagnostic signatures of the disease. A statistical approach based on combinatorial imaging was also applied for identifying the minimum set of Chl-F images, out of all those captured during the irradiation protocol, that maximise the contrast between infected and healthy tissues (Matouš et al. 2006). Using this approach, Berger et al. (2007) monitored the spread of bacterial infection in *Arabidopsis thaliana* during the very early phase of pathogen growth.

Materials and methods

Plant material

A set of 13 plants of *V. vinifera* 'Chardonnay' were obtained by vegetative propagation and cultivation in potted-soil using standard commercial substrate (65% white peat, 35% black peat, 225 g l^{-1} N, 255 g l^{-1} P_2O_5, 290 g l^{-1} K_2O, pH=5.8). Plants were maintained in a glasshouse at 25°C from April through until May 2007 (Udine, north-eastern Italy, 46° 02′ N; 13° 13′ E), without supplementary light. Two shoots per plant were grown. At the 10-leaf stage, the plants were transferred to a growth chamber and allowed to acclimatise to the most favourable conditions for infection, 2 days before inoculation (Fitotron Sanyo Gallenkamp SGC 170 PHX-J; 16/8 h light/dark period, 150 μmol (photons) m^{-2} s^{-1}, 23°C, 90–95% RH). The same conditions were maintained after inoculation for the entire course of the experiment for facilitating pathogen growth, until the occurrence of sporulation.

Plasmopara viticola inoculum

Sporangia of *P. viticola* were isolated from natural infections in the vineyards at the Experimental Farm of the University of Udine, north-eastern Italy. Leaves were detached from susceptible cultivars at the stage of oil spot symptom and incubated overnight at 20°C and 100% RH in the dark. Sporulating lesions were dried out for 2 h. Sporangia were collected with a vacuum pump into 1 ml filter tips and stored at -20°C. Sporangia were re-hydrated with distilled water at 4°C for 2 h prior to inoculation and diluted to 50,000 sporangia ml^{-1}. Viability of the released zoospores was checked by visual inspection with a stereomicroscope.

Artificial inoculation

From a total of 13 plants used as biological replicates, 10 plants were inoculated with the pathogen and three plants were used as controls. Of the three controls, two plants were inoculated with distilled water (mock-inoculated plants) and one plant was not inoculated at all.

The fourth fully expanded leaf was inoculated on one shoot per plant. Since *P. viticola* structures break through and exit the mesophyll only through the stomata in the abaxial epidermis (Fig. 1a), the shoot was positioned on a horizontal surface and the leaf laid flat with the abaxial lamina upwards. Droplets of 30 μl of zoospore suspension were applied on the abaxial side of the leaf, in the area to the right of the middle vein (Fig. 1c). Surfactants were not used in order to avoid interference with fungal growth. After

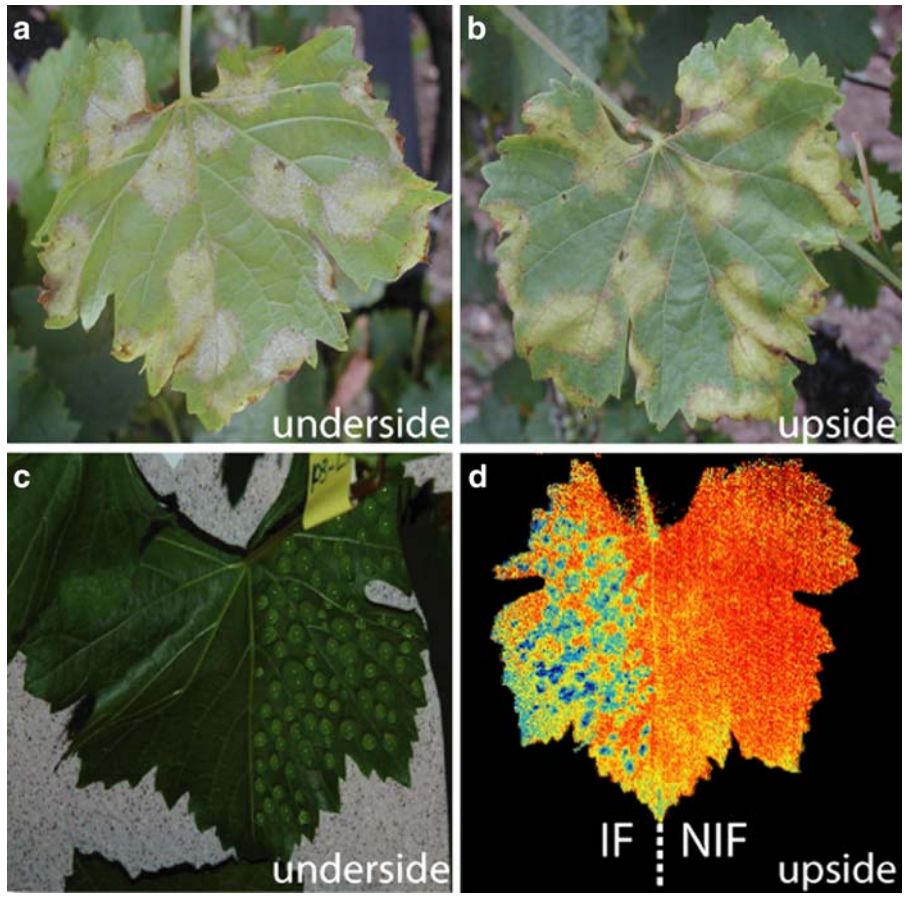

Fig. 1 Inoculation of a grapevine leaf with droplets of *P. viticola* zoospore suspension and Chl-F measurements. Under natural conditions, *P. viticola* germinating zoospores and sporangiophores are able to access and exit the mesophyll only through the stomata of the abaxial epidermis (**a**) and the developing disease is visible on the adaxial epidermis (**b**). In this experiment, the inoculum was deposited on the right half of the abaxial surface of the leaf blade, laid flat on a horizontal surface (**c**). After stomatal penetration, the droplets were dried out and the inoculated vines were returned to a growing chamber. Chl-F measurements were taken daily by exposing the adaxial epidermis to the CCD camera (**d**). Half of the inoculated leaf at the left-hand side (**d**) was analysed as the infected area (IF) and the right half as the non-infected area (NIF)

overnight incubation at 22°C, the droplets of zoospore suspension or distilled water were dried out using a napkin. Plants were then maintained in the growth chamber for 9 days and the progress of infection monitored. The appearance of visible symptoms was inspected daily from 1 to 9 days post-inoculation (dpi) on both sides of the leaf blade. Since the earliest visible symptom appears on the adaxial epidermis in the form of chlorotic spots (Fig. 1b), Chl-F was measured from the adaxial side of leaves; hence, the left side of the leaf image was analysed as infected area (IF) in the Chl-F images and the right side as non-infected area (NIF) (Fig. 1d). The infected half of the leaf was segmented and the mesophyll-invaded areas (MIF) were identified as the leaf sectors surrounding the infected spots where the infection culminated in the expression of visible symptoms. Non-inoculated halves of infected leaves, mock-inoculated leaves and leaves of the non-inoculated plants were analysed as controls.

Chlorophyll fluorescence imaging

Chl-F measurements were performed using a commercial kinetic imaging fluorometer (Open FluorCam 700 MF, Photons Systems Instruments, Ltd., Brno, Czech Republic; Nedbal et al. 2000). Chl-F emission was excited by two panels of light-emitting diodes

(LEDs, $\lambda_{max} \approx 635$ nm) that generate short measuring flashes (10 μs) and actinic light. Saturating light pulses (1,500 μmol (photons) m^{-2} s^{-1}, 1 s) were generated by a 250 W halogen lamp (λ=400–700 nm). Chl-F transients were captured by a charged coupled device (CCD) camera in a series of images with 12-bits resolution in 512×512 pixels, acquiring 50 images s^{-1}.

Chl-F transients from grapevine leaves were elicited by the irradiation protocol reported in Fig. 2. All measurements were carried out on attached leaves. Leaves were dark-adapted for 20 min, and then five measuring flashes were applied to measure minimum Chl-F in dark (F_0), when the plastoquinone pool is fully oxidised. A short saturating flash of white light (1 s, 1500 μmol (photons) m^{-2} s^{-1}) was used to reduce the plastoquinone pool and to measure maximum Chl-F (F_M). After a short dark relaxation (16 s), the leaf was exposed to low actinic light (LL, 50 μmol (photons) m^{-2} s^{-1}) for 100 s and the Kautsky effect (also known as Chl-F transient, Kautsky and Hirsch 1931; Schreiber et al. 1986) was recorded. Two saturating pulses (1,500 μmol (photons) m^{-2} s^{-1}), at 2 s and 90 s after the exposure to actinic light were applied for measuring F_{M1}' and F_{M2}', respectively, and for estimating the light-induced Chl-F quenching. A short dark adaptation (16 s) followed by two additional saturating pulses (5 s-F_{M3}' and 16 s-F_{M4}' after switching off the actinic light) was used to measure non-photochemical quenching (NPQ) recovery. These measurements were repeated after 600 s of dark-adaptation using an identical sequence of high light (HL, 200 μmol (photons) m^{-2} s^{-1}).

Analysis of standard parameters of chlorophyll fluorescence and combinatorial imaging

Images of various conventional Chl-F parameters with known physiological interpretation were inspected (e.g., F_0, F_M, F_S, F_V/F_M, Φ_{PSII}, NPQ; for description see Roháček 2002) to assess whether they displayed differences between IF, NIF and MIF areas, in particular, Chl-F parameters related to photochemical processes (maximum quantum yield of PSII, effective quantum yield of PSII in each saturating pulse both in LL and HL) and to non-photochemical quenching. The parameters were calculated as follows: $F_V/F_M = (F_M-F_0) / F_M$ (Kitajima and Butler 1975); $\Phi_{PSII} = (F_M' - F_t) / F_M'$ (Genty et al. 1989); $NPQ = (F_M - F_M') / F_M'$ (Bilger & Björkman 1990). The F_t values corresponded to Chl-F yields captured just before each saturating flash in LL and in HL.

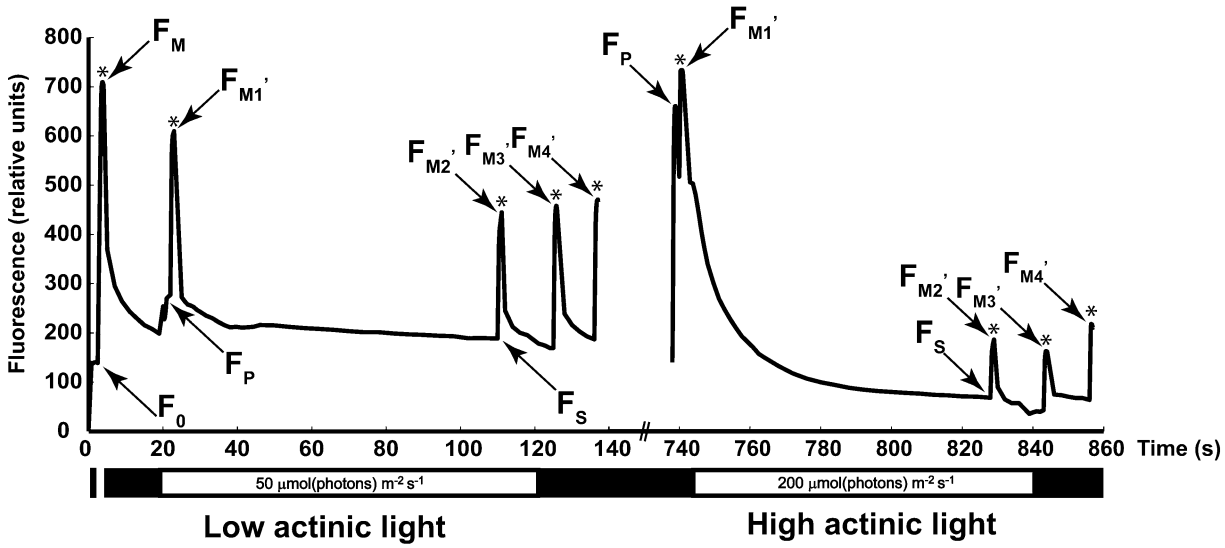

Fig. 2 Chlorophyll fluorescence (Chl-F) transients of grapevine leaves induced by a irradiating protocol of low actinic light (50 μmol (photons) m^{-2} s^{-1}) from t=0 s to t=140 s and high actinic light (200 μmol (photons) m^{-2} s^{-1}), from t=740 s to t=860 s, separated by 600 s of dark adaptation. Asterisks indicate the application of saturating flashes (1 s, 1500 μmol (photons) m^{-2} s^{-1}). Chl-F measurements (F_0, F_M, $F_{M1'}$, $F_{M2'}$, $F_{M3'}$, $F_{M4'}$, F_S) are indicated by arrows. F_0 and F_M are minimum and maximum Chl-F yield in the dark-adapted state, $F_{M1'}$, $F_{M2'}$, $F_{M3'}$, $F_{M4'}$ indicate maximum Chl-F yield in the light-adapted state measured at the 1st, 2nd, 3rd and 4th saturating pulse, F_S is the steady-state Chl-F yield in the light-adapted state

Chl-F transients captured in LL and HL of infected and control leaves were obtained by integrating signals from the centres of the leaves that were homogeneously irradiated, corresponding to a circular area of approximately 7 cm diam. This area equally included a segment from the inoculated half (IF area) and a segment from the control half of the lamina (NIF area). A non-parametric Kruskal-Wallis test was run to test the equality of population medians between Chl-F of infected and control leaves, and also among the groups of pixels in the IF, NIF and MIF segments.

Selection of small sets of Chl-F images that yielded the highest contrast between infected and healthy leaf tissue was performed using the sequentional forward floating search (SFFS) algorithm (Pudil et al. 1994) as described in detail by Matouš et al. (2006). The algorithm was initially calibrated using a training data set based on Chl-F data generated through the entire experiment from segments of the leaves that were either certainly infected or sampled from the non-inoculated controls. This process aided the algorithm to interpret how Chl-F is affected by the infection, and made use of Chl-F data from the end of the experiment after visible symptoms appeared (at 7 dpi, late phase of the infection), from the middle of the experiment when the symptoms were detectable only by standard Chl-F parameters (from 4 to 6 dpi, middle phase of the infection) and from the beginning of the experiment when the pixels corresponding to the infected spots of the leaf were presumed on the basis of the position of the visible symptoms in later phases (from 1 to 3 dpi, early phase of the infection).

A set of Chl-F images that yielded maximum contrast between MIF and NIF areas in the late, middle and early phase was identified. During this process, any selected pixel in the tested Chl-F image was compared to homologous training sets of images from the MIF and NIF tissues. If the Chl-F level of the pixel was more similar to that of the MIF tissue, the pixel was classified as infected, otherwise it was classified as non-infected. The *a priori* knowledge of the position of this particular pixel and to which kind of tissue it belonged to (MIF or NIF) was used to decide if the classification was correct or erroneous. The performance parameter $P=(N–M)/(N + M)$, where N are correct pixel classifications and M are false classifications, was used to estimate the contrast provided by each image. The subset of *j* Chl-F images that yielded the lowest error rate and therefore the highest contrast between the MIF and NIF segments was chosen by the iterative process of image selection perfomed by the SFFS algorithm. Finally, a combinatorial imaging (CI) parameter was calculated for each pixel using the Linear Discriminant Analysis algorithm (Fukunaga 1990) and the combination of the most contrasting images previously identified by the SFFS alorithm. The resulting CI parameter was used for generating a CI image of the leaf in false colour scale.

Results

Visible symptoms

The first visible symptom appeared at 7 dpi in the IF half of the leaves, in the form of chlorotic oil spots that were noticeable through the upperside of the epidermis (Fig. 3). Chlorotic oil spots corresponded to the leaf segments where the droplets of inoculum were deposited on the underside of the lamina. Sporangiophores emerged from the stomata of the abaxial lamina underneath the oil spots and produced sporangia at 9 dpi. Soon after the final stage of pathogen asexual reproduction had been achieved, the experiment was interrupted and the sporulating lesions developed necrosis. Neither downy mildew symptoms nor physiological stresses were observed in the NIF half of the inoculated leaves, in the mock-inoculated leaves or in the non-inoculated leaves, incubated under the same conditions as the inoculated plants for the entire duration of the experiment.

Imaging of standard Chl-F parameters

Chl-F parameters related to photosynthetic activity of leaves (F_V/F_M and Φ_{PSII}) were more effective in detecting *P. viticola* infection in grapevine leaves than other conventional parameters, i.e. NPQ. The most contrasting F_V/F_M and Φ_{PSII} images of a representative infected leaf during the progression of infection are shown in Fig. 4. The earliest change of the F_V/F_M pattern appeared at 4 dpi (Fig. 4a) as circular areas with lower F_V/F_M values in the half of the leaf where the fungus was inoculated. The infected spots expressed F_V/F_M values of 0.76 at 4 dpi, and then the signals further decreased to the lowest value (0.71) at 7 dpi. F_V/F_M values across the non-infected tissue in the right

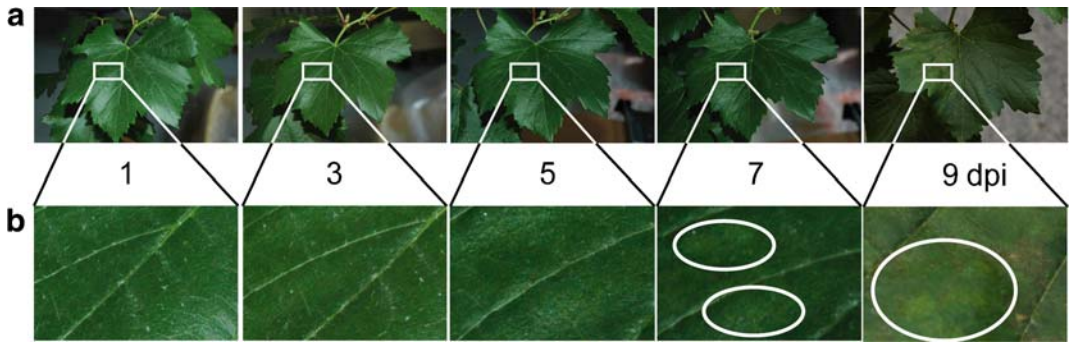

Fig. 3 Visible symptoms of downy mildew in grapevine leaves infected with *P. viticola*. (**a**) Adaxial blade of a representative grapevine leaf at 1, 3, 5, 7 and 9 dpi, inoculated in the area to the left of the middle vein. (**b**) Magnification of the inoculated area. The first symptoms were barely visible at 7 dpi as oil spots and they are indicated by white ellipses. Chlorotic areas became more evident at 9 dpi

half of the leaves remained >0.8, at values that are usually associated with optimal photosynthetic performance (Björkman and Demmig 1987). Similar values of F_V/F_M (>0.8) were homogeneously recorded across whole mock-inoculated leaves and across leaves of the non-inoculated controls during the entire course of the experiment (Fig. 5).

The Φ_{PSII} images of infected leaves taken at the second, third and fourth pulse in LL and in HL displayed Chl-F patterns similar to those obtained with F_V/F_M images. The most contrasting image for distinguishing healthy and infected tissues was taken at the second pulse in HL (i.e., at light-adapted 'steady state' condition) ($\Phi_{PSII\text{-}HL}$, Fig. 4b). $\Phi_{PSII\text{-}HL}$ images displayed the first evidence of infection at 4 dpi, and the evolution during the progress of the infection was reminiscent of that displayed by F_V/F_M. $\Phi_{PSII\text{-}HL}$ values decreased in the infected spots from 0.25 at 4 dpi to 0.19 at 7 dpi. NIF area, mock-inoculated leaves, and negative controls exhibited homogeneously-distributed $\Phi_{PSII\text{-}HL}$ signals across the lamina in the range of 0.42–0.46.

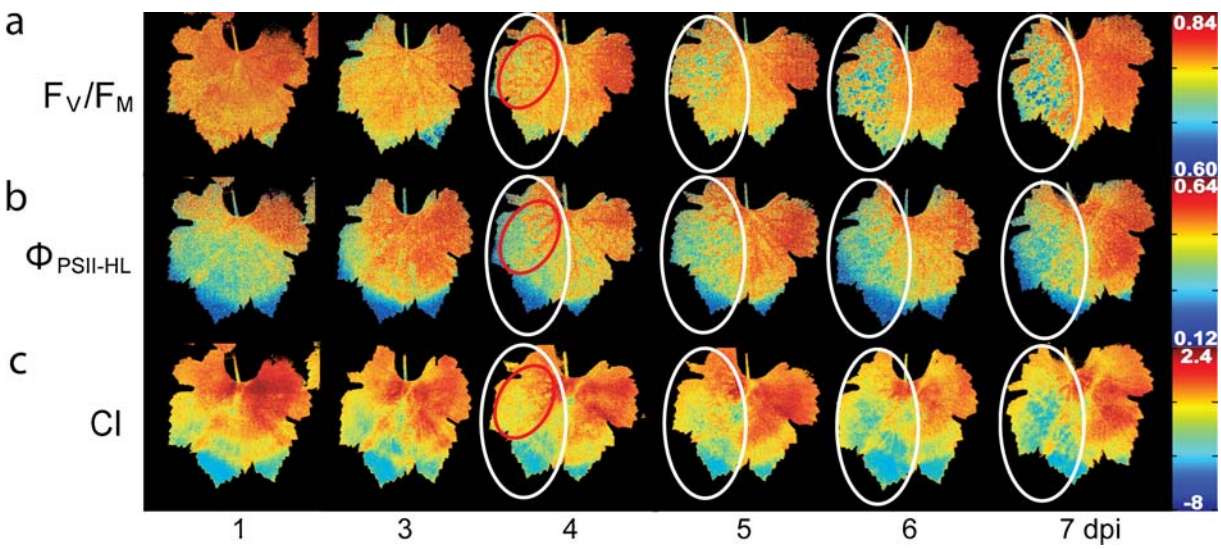

Fig. 4 False-colour images of (**a**) maximum quantum yield of photosystem II (F_V/F_M), (**b**) effective quantum yield of photosystem II in high actinic light ($\Phi_{PSII\text{-}HL}$) and (**c**) combinatorial imaging parameter (CI) of a representative grapevine leaf during the course of *P. viticola* infection, from 1 dpi until the appearance of the first visible symptoms at 7 dpi. White ellipses indicate the leaf area inoculated with *P. viticola*. Red circles indicate the leaf areas, in which the first symptoms of the infection occurred. The colour scale with minimum and maximum values for each Chl-F parameter is reported at the right-hand side

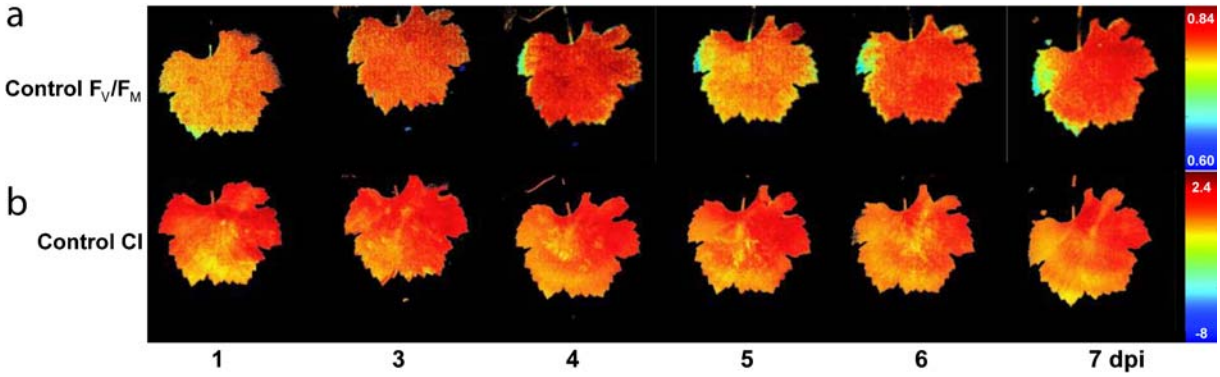

Fig. 5 Images of (**a**) maximum quantum yield of photosystem II (F_V/F_M) and (**b**) the combinatorial imaging (CI) parameter in control leaves during the course of the experiment. The colour scale with minimum and maximum values for each Chl-F parameter is reported at the right-hand side

Combinatorial imaging

A combinatorial imaging method was applied to the entire series of captured Chl-F images during the measuring protocol (Matouš et al. 2006). A combination of seven Chl-F images that maximise the contrast between the inoculated part of the leaf and controls was identified. These seven images were taken in the interval between 2.4 s to 743 s of the protocol (Fig. 2). The linear combination of these Chl-F measurements was: CI=−0.21 F(t=2.4 s) - 0.22 F(t=5 s)+0.39 F(t=41.2 s) - 0.22 F(t=126 s)+0.09 F(t=738 s)+0.83 F(t=740 s) - 0.10 F(t=743 s). CI is an artificial parameter without any physiological meaning, which aimed only at disclosing the maximum contrast between infected and healthy tissues. The CI images were drawn by calculating CI pixel-by-pixel according to above-mentioned equation and shown in false colour scale (Fig. 4c). CI images revealed the first signatures of *P. viticola* infection at 4 dpi, at the same stage of disease progression that conventional Chl-F parameters manifested the differences between healthy and infected tissues. Control leaves expressed homogeneous CI levels over the whole leaf area (Fig. 5).

Integral analysis of chlorophyll fluorescence parameters

No statistical difference was found between the overall mean of Chl-F signals from infected leaves and controls (Fig. 6), probably because the signal of infected spots of leaves was overshadowed by the signal of the intervening healthy non-infected parts. It can be argued that the alteration of photosynthesis caused by the infection was localised to the invaded area and, since the host genotype is completely susceptible to the pathogen, the plant did not mount any systemic defence reaction in response to the infection.

Since the zoospores are motile only in water and hyphae of *P. viticola* can not penetrate the veins in the mesophyll, mycelial growth is constrained in the intercostal field of the mesophyll on which each droplet of inoculum was deposited (Unger et al. 2007). Thus, the mean Chl-F signal of the leaf spots directly invaded by the pathogen within the infected half (MIF) was calculated and compared with the mean Chl-F signal from the whole infected half (IF) and the non-infected half (NIF).

Time-course of the standard Chl-F parameters F_0, F_S in HL, F_V/F_M and $\Phi_{PSII\text{-}HL}$ in IF, MIF and NIF area is reported in Fig. 6. No statistical difference was obtained between leaves of control plants and the NIF half of the infected leaves for any of the tested parameters. Hence, the Chl-F signal of the NIF half of inoculated leaves was then used as the negative control for statistical analysis. The difference between Chl-F of the NIF and the IF areas was not significant (Fig. 6). By contrast, significant differences were found between the MIF and the NIF area for F_V/F_M and $\Phi_{PSII\text{-}HL}$ at 5 dpi and 6 dpi, respectively (Fig. 6c, d). The significant variations of these Chl-F parameters were caused by an increase of minimal Chl-F measured in a dark-adapted state (F_0, Fig. 6a) and steady-state Chl-F in a light-adapted state (F_S, Fig. 6b) in the MIF

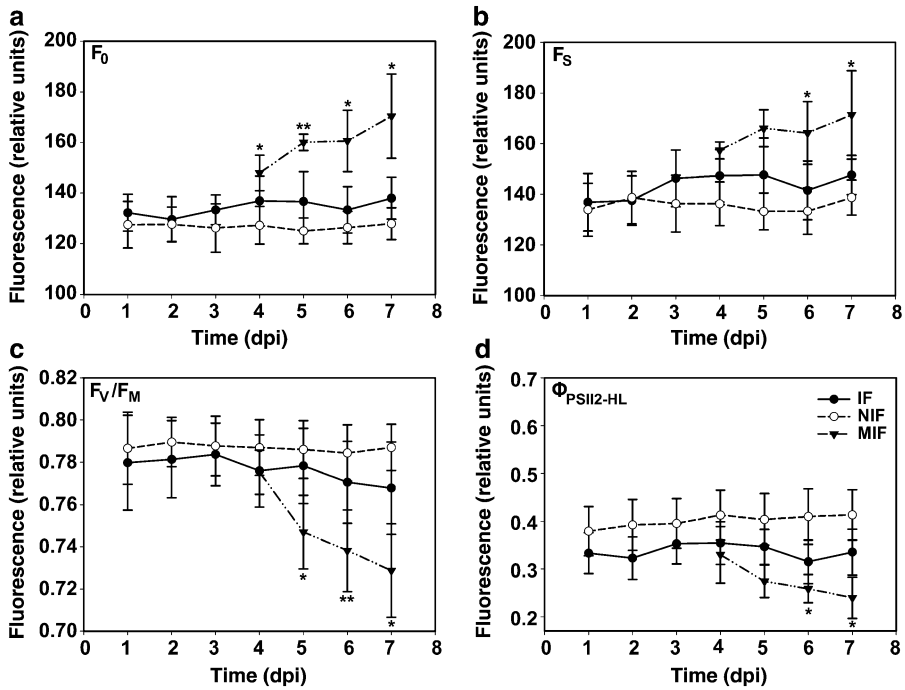

Fig. 6 Time-course of standard Chl-F parameters such as (**a**) minimum Chl-F yield in the dark-adapted state (F_0), (**b**) steady-state Chl-F yield in the light-adapted state (F_S), (**c**) maximum quantum yield of photosystem II (F_V/F_M) and (**d**) effective quantum yield of photosystem II in high actinic light ($\Phi_{PSII-HL}$) calculated over the non-infected half (NIF, solid line), over the infected half (IF, dashed line) of the inoculated leaves and in the spots of the mesophyll invaded by the pathogen within the inoculated half (MIF, dash-dotted line) where disease symptoms became visible at 7 dpi. Each data point represents the average of 10 measurements. Bars represent standard deviations. Asterisks stand for significant differences between MIF and NIF areas at $P<0.05$ (*) and $P<0.01$ (**), according to a Kruskal-Wallis test

area during the middle stages of disease incubation, which are the factors included in the calculation of the derived parameters F_V/F_M and $\Phi_{PSII-HL}$. The increase of F_0 and F_S would indicate a disconnection of the light-harvesting antennae from the reaction centres. At the latest phases of infection (7 and 9 dpi), F_V/F_M and $\Phi_{PSII-HL}$ also decreased because maximum Chl-F yields (F_M in dark, $F_{M'}$ in light) decreased as a probable result of chlorophyll degradation in the infected leaf segments.

Quantitation of the leaf area infected by *P. viticola* based on chlorophyll fluorescence images

The F_V/F_M and $\Phi_{PSII2HL}$ images of the IF half of the leaves were segmented by pixel-by-pixel analysis and the size of the infected area was defined. Spatial resolution of Chl-F imaging allowed calculation of the daily progress of the infected area over the course of disease incubation (Table 1). In this experimental model, in which inoculum was deposited as droplets of zoospore suspension, the leaf area infected at the latest phase of the incubation period (7 dpi) was 20.9% of the lamina based on F_V/F_M images and 35.7% based on $\Phi_{PSII-HL}$ images. The disease was not manifested until 3 dpi. At 4 dpi, the patches of the leaves in which F_V/F_M and $\Phi_{PSII-HL}$ were affected already covered 17.1% and 26.2% of the IF area, respectively.

Discussion

Chl-F imaging has been broadly applied to study biotic stress in plants (Nedbal and Whitmarsh 2004) and to detect physiological alterations induced in infected plant tissue (Lichtenthaler and Miehé 1997). In this study, conventional and combinatorial Chl-F imaging of leaf tissue was used to detect *P. viticola* infection inside grapevine leaves, utilising Chl-F

Table 1 Mesophyll invaded area (MIF) within the inoculated half of the leaf (IF) estimated by pixel counting using images of maximum quantum yield of photosystem II (F_V/F_M) and effective quantum yield of photosystem II in high actinic light ($\Phi_{PSII\text{-}HL}$)

	F_V/F_M			$\Phi_{PSII\text{-}HL}$		
DPI	IF area	MIF area	%MIF area	IF area	MIF area	%MIF area
0	53,021	0	0	53;019	0	0
1	50,344	0	0	50,339	0	0
2	51,609	0	0	51,608	0	0
3	57,350	200	0.3	57,345	582	1.0
4	52,993	9,050	17.1	52,992	13,912	26.2
5	54,630	11,325	20.7	54,626	16,718	30.6
6	54,001	13,155	24.4	53,995	19,787	36.6
7	54,329	11,378	20.9	51,272	18,289	35.7

parameters that would reveal the infection as early as possible and that could be measured in the field. Two standard Chl-F parameters that have physiological interpretation, maximum and effective quantum yield (F_V/F_M and $\Phi_{PSII;}$ Kitajima and Butler 1975; Genty et al. 1989), met the above-mentioned requirements. These Chl-F parameters report on perturbations in photosynthetic efficiency of PSII that are specifically associated with the spots in which the disease is developing. One major advantage of the Φ_{PSII} parameter is the possibility of being measured in sunlight, in leaves in light-adapted states, while measurement of F_V/F_M requires dark adaptation of leaves. Both parameters revealed the first signature of the infection at 4 dpi by a significant decrease of Chl-F values in the spots where *P. viticola* had been inoculated. This prediction was effective 3 days earlier than the appearance of any visible symptoms and 5 days before the completion of the pathogen's asexual cycle, which culminated with the release of sporangia. The application of a combinatorial imaging method did not allow earlier detection of the infected areas. The CI parameter performed in a similar way as F_V/F_M and $\Phi_{PSII\text{-}HL}$.

Plasmopara viticola infection did not cause detectable effects on leaf photosynthesis outside of the area invaded by the pathogen, since no significant changes of Chl-F parameters were observed in the non-inoculated half of the leaf challenged with the pathogen. The area in which photosynthetic efficiency was affected was negligible until 30% of the incubation period. The area affected by the pathogen expanded rapidly between 3 and 5 dpi, at around 50% of the incubation period. This disease progression is consistent with previous reports on the growth of *P. viticola* in attached leaves during the initial phase of the plant-pathogen interaction (Unger et al. 2007). At the latest phase of the infection (7–9 dpi), the negative effect on photosynthesis remained restricted to the intercostal fields of the lamina where the pathogen had entered the mesophyll. This evidence confirmed previous histochemical observations that veins are physical barriers against spatial invasion of the mesophyll by *P. viticola* (Unger et al. 2007). Field empirical observations are also in accordance with this finding. Thus, imaging of F_V/F_M or Φ_{PSII} heterogeneity in leaf lamina can be used for the early assessment of developing infection in the field. This tool may assist in the decision of spraying chemicals only when necessary, before substantial damage is caused, and before the pathogen spreads through sporulation.

Leaf area with lowered Φ_{PSII} was larger than the area with lowered F_V/F_M. The heterogeneity of Φ_{PSII} indicates leaf segments where photochemical energy conversion in PSII is impaired, which is often correlated with the yield of CO_2 fixation (Genty et al. 1989), while decline of the F_V/F_M parameter reports on the injury of PSII complexes (Bilger and Björkman 1990). Thus, imaging of Φ_{PSII} distribution across leaf lamina would provide growers with a more conservative estimate of how much the plant is suffering from the infection.

Two major advantages of Chl-F imaging over alternative techniques (Allègre et al. 2007) are the sensitivity and the high spatial resolution (reviewed by Nedbal and Whitmarsh 2004). These two features are not dispensable for a successful detection of *P. viticola* in grapevine leaves at early stages of infection, and they are currently provided only by sophisticated CCD cameras. This limitation would hamper a comfortable

use of Chl-F imaging in the field. Fast and effective screening of *P. viticola* infection in the vineyards would thus require the transfer of this technology to portable and user-friendly devices.

Chl-F imaging could also help in the large-scale screening of quantitative resistance of grapevine plants to *P. viticola*. Experimental progenies are bred by mating resistant and susceptible grapes and usually exhibit a continuous variation for severity of infection. While major genes were found (Welter et al. 2007), the identification of genes committed to minor effects on resistance is hampered by the lack of accurate methods for automated phenotyping, that is, quantifying the area invaded by the pathogen precisely and promptly across thousands of seedlings. F_V/F_M and Φ_{PSII} images would provide powerful tools for measuring the infected area, compared to current methods of visualisation of *P. viticola* mycelium within the mesophyll based on histochemistry (Kortekamp 2005; Díez-Navajas et al. 2007).

In summary, heterogeneous distribution of Chl-F across grapevine leaves is a diagnostic tool for early detection of *P. viticola* infection. Maximum and effective quantum yields of PSII revealed the infection 3 days before the appearance of visible symptoms. *Plasmopara viticola* did not spread systemically outside the inoculated area and the susceptible host genotype did not mount systemic responses against the pathogen infection. Hence, Chl-F did not change outside the spots of inoculation. The Chl-F imaging method therefore requires high spatial resolution for revealing the earliest stages of the infection.

Acknowledgements This work was supported by grants AV0Z60870520 (ISBE ASCR), 2B06068 (ISBE ASCR) and MSM6007665808 (IPB USB) awarded by the Academy of Sciences of the Czech Republic and Ministry of Education, Youth and Sports of the Czech Republic, and also funded by the Regional Administration of Friuli Venezia Giulia (Italy). The published data resulted also from preliminary experiments for the project 522/09/1565 funded by the Academy of Sciences of the Czech Republic. The authors thank Vítězslav Březina for advice in statistical analysis and Courtney Coleman for proof reading.

References

Allègre, M., Daire, X., Héloir, M. C., Trouvelot, S., Mercier, L., Adrian, M., et al. (2007). Stomatal deregulation in *Plasmopara viticola*-infected grapevine leaves. *The New Phytologist, 173*, 832–840. doi:10.1111/j.1469-8137.2006.01959.x.

Barbagallo, R. P., Oxborough, K., Pallett, K. E., & Baker, N. R. (2003). Rapid, noninvasive screening for perturbations of metabolism and plant growth using chlorophyll fluorescence imaging. *Plant Physiology, 132*, 485–493. doi:10.1104/pp.102.018093.

Berger, S., Benediktyová, Z., Matouš, K., Benfig, K., Mueller, M. J., Nedbal, L., et al. (2007). Visualization of dynamics of plant-pathogen interaction by novel combination of chlorophyll fluorescence imaging and statistical analysis: differential effects of virulent and avirulent strains of *P. syringae* and of oxylipins on *A. thaliana*. *Journal of Experimental Botany, 58*, 797–806. doi:10.1093/jxb/erl208.

Bilger, W., & Björkman, O. (1990). Role of the xantophyll cycle in photoprotection elucidated by measurements of light-induced absorbance changes, fluorescence and photosynthesis in *Hedera canariensis*. *Photosynthesis Research, 25*, 173–185. doi:10.1007/BF00033159.

Björkman, O., & Demmig, B. (1987). Photon yield of O2–evolution and chlorophyll fluorescence characterization at 77 K among vascular plants of diverse origin. *Planta, 170*, 489–504. doi:10.1007/BF00402983.

Bugliosi, R., Spera, G., La Torre, A., Campoli, L., Gianferro, M., & Talocci, S. (2007). A two years study results in the use of artificial neural networks to forecast *Plasmopara viticola* infection in viticulture. *Communications in Agricultural and Applied Biological Sciences*, *72*, 321–325.

Chaerle, L., & Van Der Straeten, D. (2001). Seeing is believing: imaging techniques to monitor plant health. *Biochimica et Biophysica Acta, 1519*, 153–166.

Chou, H.-M., Bundock, N., Rolfe, S. A., & Scholes, J. D. (2000). Infection of *Arabidopsis thaliana* leaves with *Albugo candida* (white blister rust) causes a reprogramming of host metabolism. *Molecular Plant Pathology, 1*, 99–113. doi:10.1046/j.1364-3703.2000.00013.x.

Díez-Navajas, A. M., Greif, C., Poutaraud, A., & Merdinoglu, D. (2007). Two simplified fluorescent staining techniques to observe infection structures of the oomycete *Plasmopara viticola* in grapevine leaf tissues. *Micron (Oxford, England), 38*, 680–683. doi:10.1016/j.micron.2006.09.009.

Emmett, R. W., Wicks, T. J., & Magarey, P. A. (1992). Downy mildew of grapes. In J. Kumar, H. S. Chaube, U. S. Singh & A. N. Mukhopadhyay (Eds.), *Plant diseases of international importance. Vol II: Diseases of fruit crops*, pp. 90–128. Englewood Cliffs: Prentice Hall.

Eurostat report. (2007). *The use of plant protection products in the European Union. Data 1992–2003*. Luxembourg: Eurostat European Commission.

Fukunaga, K. (1990). *Introduction to statistical pattern recognition*. New York: Academic.

Genty, B., Briantais, J.-M., & Baker, N. R. (1989). The relationship between quantum yield of photosynthetic electron transport and quenching of chlorophyll fluorescence. *Biochimica et Biophysica Acta, 990*, 87–92.

Jaillon, O., Aury, J.-M., Noel, B., Policriti, A., Clepet, C., et al. (2007). The grapevine genome sequence suggests ancestral hexaploidization in major angiosperm phyla. *Nature, 449*, 463–468. doi:10.1038/nature06148.

Kautsky, H., & Hirsch, A. (1931). Neue Versuche zur Kohlensäureassimilation. *Naturwissenschaften, 48*, 964–964. doi:10.1007/BF01516164.

Kitajima, M., & Butler, W. L. (1975). Quenching of chlorophyll fluorescence and primary photochemistry in chloroplasts by dibromothymoquinone. *Biochimica et Biophysica Acta, 376*, 105–115. doi:10.1016/0005-2728(75)90209-1.

Kortekamp, A. (2005). Growth, occurrence and development of septa in *Plasmopara viticola* and other members of the Peronosporaceae using light— and epifluorescence-microscopy. *Mycological Research, 109*, 640–648. doi:10.1017/S0953756205002418.

La Torre, A., Spera, G., & Lolletti, D. (2005). Grapevine downy mildew control in organic farming. *Communications in Agricultural and Applied Biological Sciences, 70*, 371–379.

Lichtenthaler, H. K., & Miehé, J. A. (1997). Fluorescence imaging as a diagnostic tool for plant stress. *Trends in Plant Science, 2*, 316–320. doi:10.1016/S1360-1385(97)89954-2.

Matouš, K., Benediktyová, Z., Berger, S., Roitsch, T., & Nedbal, L. (2006). Case study of combinatorial imaging: what protocol and what chlorophyll fluorescence image to use when visualizing infection of *Arabidopsis thaliana* by *Pseudomonas syringae?*. *Photosynthesis Research, 90*, 243–253. doi:10.1007/s11120-006-9120-6.

Meyer, S., Saccardy-Adji, K., Rizza, F., & Genty, B. (2001). Inhibition of photosynthesis by *Colletotrichum lindemuthianum* in bean leaves determined by chlorophyll fluorescence imaging. *Plant, Cell & Environment, 24*, 947–955. doi:10.1046/j.0016-8025.2001.00737.x.

Nedbal, L., & Whitmarsh, J. (2004). Chlorophyll fluorescence imaging of leaves and fruits. In C. G. Papageorgiou & C. G. Govindjee (Eds.), *Chlorophyll a fluorescence: A signature photosynthesis*, pp. 389–407. Dordrecht: Springer.

Nedbal, L., Soukupová, J., Kaftan, D., Whitmarsh, J., & Trtílek, M. (2000). Kinetic imaging of chlorophyll fluorescence using modulated light. *Photosynthesis Research, 66*, 3–12. doi:10.1023/A:1010729821876.

Omasa, K., Shimazaki, K.-I., Aiga, I., Larcher, W., & Onoe, M. (1987). Image analysis of chlorophyll fluorescence transients for diagnosing the photosynthetic system of attached leaves. *Plant Physiology, 84*, 748–752. doi:10.1104/pp. 84.3.748.

Papageorgiou, C. G. & Govindjee (Eds.) (2004). *Chlorophyll a fluorescence: A signature photosynthesis*. Dordrecht: Springer

Polesani, M., Desario, F., Ferrarini, A., Zamboni, A., Pezzotti, M., Kortekamp, A., et al. (2008). cDNA-AFLP analysis of plant and pathogen genes expressed in grapevine infected with *Plasmopara viticola*. *BMC Genomics, 9*, 142. doi:10.1186/1471-2164-9-142.

Pudil, P., Novovičová, J., & Kittler, J. (1994). Floating search methods in feature selection. *Pattern Recognition Letters, 15*, 1119–1125. doi:10.1016/0167-8655(94)90127-9.

Rodríguez-Moreno, L., Pineda, M., Soukupová, J., Macho, A. P., Beuzón, C. R., Barón, M., et al. (2008). Early detection of bean infection by *Pseudomonas syringae* in asymptomatic leaf areas using chlorophyll fluorescence imaging. *Photosynthesis Research, 96*, 27–35. doi:10.1007/s11120-007-9278-6.

Roháček, K. (2002). Chlorophyll fluorescence parameters: the definitions, photosynthetic meaning, and mutual relationships. *Photosynthetica, 40*, 13–29. doi:10.1023/A:1020125719386.

Scharte, J., Schon, H., & Weis, E. (2005). Photosynthesis and carbohydrate metabolism in tobacco leaves during an incompatible interaction with *Phytophthora nicotianae*. *Plant, Cell & Environment, 28*, 1421–1435. doi:10.1111/j.1365-3040.2005.01380.x.

Scholes, J. D., & Rolfe, S. A. (1996). Photosynthesis in localised regions of oat leaves infected with crown rust (*Puccinia coronata*): quantitative imaging of chlorophyll fluorescence. *Planta, 199*, 573–582. doi:10.1007/BF00195189.

Schreiber, U., Schliwa, U., & Bilger, W. (1986). Continuous recording of photochemical and nonphotochemical chlorophyll fluorescence quenching with a new type of modulation fluorometer. *Photosynthesis Research, 10*, 51–62. doi:10.1007/BF00024185.

Spera, G., La Torre, A., & Alegi, S. (2003). Organic viticulture: efficacy evaluation of different fungicides against *Plasmopara viticola*. *Communications in Agricultural and Applied Biological Sciences, 68*, 837–847.

Soukupová, J., Smatanová, S., Nedbal, L., & Jegorov, A. (2003). Plant response to destruxins visualized by imaging of chlorophyll fluorescence. *Physiologia Plantarum, 118*, 399–405. doi:10.1034/j.1399-3054.2003.00119.x.

Swarbrick, P. J., Schulze-Lefert, P., & Scholes, J. D. (2006). Metabolic consequences of susceptibility and resistance (race-specific and broad-spectrum) in barley leaves challenged with powdery mildew. *Plant, Cell & Environment, 29*, 1061–1076. doi:10.1111/j.1365-3040.2005.01472.x.

Unger, S., Büche, C., Boso, S., & Kassemeyer, H.-H. (2007). The course of colonization of two different *Vitis* genotypes by *Plasmopara viticola* indicates compatible and incompatible host-pathogen interaction. *Phytopathology, 97*, 780–786. doi:10.1094/PHYTO-97-7-0780.

Welter, L. J., Göktürk-Baydar, N., Akkurt, M., Maul, E., Eibach, R., Töpfer, R., et al. (2007). Genetic mapping and localization of quantitative trait loci affecting fungal disease resistance and leaf morphology in grapevine (*Vitis vinifera* L). *Molecular Breeding, 20*, 359–374. doi:10.1007/s11032-007-9097-7.